CrystEngComm

COMMUNICATION

View Article Online
View Journal | View Issue

Cite this: *CrystEngComm*, 2024, **26**, 6683

Received 13th October 2024,
Accepted 9th November 2024

DOI: 10.1039/d4ce01051e

rsc.li/crystengcomm

Rare-earth oxychalcogenide $Eu_2ZnGe_2OS_6$: a phase-matching infrared nonlinear optical material with $[GeOS_3]$ units†

Guili Wang,[ab] Wentian Wu,[ab] Chunxiao Li[a] and Jiyong Yao *[ab]

Oxychalcogenides have been highly anticipated as nonlinear optical (NLO) crystals because of their excellent optical properties. Herein, a rare-earth oxychalcogenide $Eu_2ZnGe_2OS_6$ was successfully designed and synthesized. It crystallizes in the non-centrosymmetric $P\bar{4}2_1m$ space group with highly polarized mixed-anion $[GeOS_3]$ units and exhibits an indirect band gap of 2.22 eV, a moderate second harmonic generation (SHG) response (0.4 × AGS), and phase-matching properties. Additionally, $Eu_2ZnGe_2OS_6$ exhibits a significant calculated birefringence of 0.173@2090 nm. This research has enriched the rarely studied rare-earth oxychalcogenide system and provided new ideas for the design of promising IR NLO crystals.

Introduction

Nonlinear optical (NLO) crystals, serving as pivotal functional materials for laser wavelength frequency conversion, effectively broaden the tunable range of lasers, thereby holding substantial significance in advancing laser technology.[1–7] Over the past decades, a series of oxygen-based NLO materials with excellent comprehensive performance have been discovered and commercially applied in the visible and ultraviolet (UV) regions, including KH_2PO_4 (KDP),[8] $KTiOPO_4$ (KTP),[9] LiB_3O_5 (LBO),[10] β-BaB_2O_4 (BBO),[11] CsB_3O_5 (CBO),[12] $CsLiB_6O_{10}$ (CLBO),[13] and $KBe_2BO_3F_2$ (KBBF).[14,15] Comparatively, the development of infrared (IR) NLO crystals is slightly behind. In the realm of IR NLO crystals, materials like $AgGaSe_2$ (AGSe),[16] $AgGaS_2$ (AGS),[17] and $ZnGeP_2$ (ZGP)[18] that have been commercialized are characterized by their significant second-harmonic generation (SHG) coefficients, broad IR transmission ranges, and excellent phase-matching (PM) properties. Nonetheless, the limitation imposed by their relatively low laser-induced damage thresholds (LIDTs) and two-photon absorption hampers their energy conversion efficiency and constrains their practical applications.[19,20]

Consequently, investigators have put forth several optimization strategies aimed at designing and fabricating high-performance IR NLO crystals. Among these, the strategy of incorporating mixed-anion units has proven to be effective due to its capacity to combine the advantageous properties of various compounds, such as the large band gaps and high LIDTs characteristic of oxides and halides, along with the substantial SHG coefficients associated with chalcogenides. In recent years, this strategy has been employed to design and synthesize oxyhalides, chalcohalides, and oxychalcogenides that exhibit promising IR NLO performance, including $Pb_{17}O_8Cl_{18}$,[21] $K_4ZnV_5O_{15}Cl$,[22] Pb_4SeBr_6,[23] $Ba_4Ge_3S_9Cl_2$,[24] $Sr_6Ge_3OSe_{11}$,[25] and $SrGeOSe_2$.[26] The strategic integration of these diverse anions facilitates the optimization of NLO properties, resulting in materials with enhanced photonic applications. In the case of oxychalcogenides, the mixed-anion functional units formed by the multiple combinations of the oxygen anion (O^{2-}) and chalcogenide anions ($Q = S^{2-}$, Se^{2-}, Te^{2-}) will generate more NLO-active building units (such as $[GeOS_3]$, $[GeO_3S]$, and $[GeO_2S_2]$ units), thereby achieving excellent NLO performance.

In this work, a new rare-earth oxychalcogenide $Eu_2ZnGe_2OS_6$ was successfully designed and synthesized through a spontaneous crystallization method, exhibiting balanced NLO properties. The crystal structure and optical properties of $Eu_2ZnGe_2OS_6$ have been extensively studied through single crystal X-ray diffraction (XRD), IR spectrum, UV-vis-NIR diffuse reflectance spectrum, Raman spectrum, and SHG tests. Concurrently, the structure–property relationship of the title compound has been unraveled through advanced theoretical calculations employing the CASTEP package based on density functional theory (DFT).

[a] *Beijing Center for Crystal Research and Development, Key Lab of Functional Crystals and Laser Technology, Technical Institute of Physics and Chemistry, Chinese Academy of Sciences, Beijing 100190, P. R. China.*
E-mail: jyao@mail.ipc.ac.cn
[b] *Center of Materials Science and Optoelectronics Engineering, University of Chinese Academy of Sciences, Beijing 100049, P. R. China*

† Electronic supplementary information (ESI) available. CCDC 2390087. For ESI and crystallographic data in CIF or other electronic format see DOI: https://doi.org/10.1039/d4ce01051e

Results and discussion

$Eu_2ZnGe_2OS_6$ is isostructural to the compounds of the $A_2MM'_2OS_6$ (A = Ca, Sr, Eu; M = Mn, Fe, Co, Zn, Cd, Hg, Ge; M′ = Ga, Ge, Sn)[27–36] family and belongs to the non-centrosymmetric (NCS) tetragonal space group $P\bar{4}2_1m$ (no. 113) with unit cell parameters of a = 9.3838(7) Å, b = 9.3838(7) Å, c = 6.1509(7) Å, and Z = 2. The crystallographic data and structure refinement for $Eu_2ZnGe_2OS_6$ are illustrated in Table S1.† In its asymmetric unit, one independent Eu atom, one independent Zn atom, one independent Ge atom, one independent O atom, and two independent S atoms with full occupancy are present. The calculated bond valence sums (BVS) of Eu1, Zn1, Ge1, S1, S2, and O1 atoms are 2.101, 2.122, 4.071, −2.156, −1.968, and −1.907, respectively, which are very similar to their corresponding ideal oxidation states (Table S2†).

The crystal structure of $Eu_2ZnGe_2OS_6$ is presented in Fig. 1. It is characterized by innumerable two-dimensional (2D) $[ZnGe_2OS_6]^{4-}$ layers extending along the *ab*-plane and $[EuOS_7]$ polyhedra located between the layers (Fig. 1(a)). These 2D layers are composed of an uncountable number of $[ZnS_4]$ tetrahedra and $[Ge_2OS_6]$ dimers interconnected by corner-sharing with S1 atoms, with the $[Ge_2OS_6]$ dimers being formed by two $[GeOS_3]$ units sharing the common O1 atoms (Fig. 1(b)). The coordination geometry of $Eu_2ZnGe_2OS_6$ is presented in Fig. S2,† and the selected bond lengths and bond angles are listed in Table S3.† Each Eu1 atom is surrounded by four S1 atoms, three S2 atoms, and one O1 atom, with an Eu–O bond length of 2.809(5) Å, which is very similar to that in $EuAl_2O_4$ [2.499(2)–3.088(14) Å].[37] The Eu–S bond with a length range of 3.0265(14)–3.1027(18) Å is very reasonable concerning that reported for $EuCdGeS_4$ (3.0106–3.1530 Å).[38] Each Zn1 atom is interconnected with four S1 atoms to form a typical tetrahedron with a Zn–S bond length of 2.3245(13) Å. Reciprocally, each Ge1 atom is surrounded by two S1 atoms, one S2 atom, and one O1 atom to form a highly distorted mixed-anion $[GeOS_3]$ unit. The Ge–S bond lengths are in the range of 2.1442(18)–2.2048(13) Å, and the Ge–O bond length is 1.837(3) Å, which are very similar to the values involved in $Ba_3S[GeOS_3]$[39] (Ge–S bond lengths: 2.207(3)–2.223(3) Å; Ge–O bond length: 1.755(7) Å) containing $[GeOS_3]$ units.

Fig. S1† illustrates the element distribution images and atomic percentage (%) of $Eu_2ZnGe_2OS_6$. This result indicates that the elements Eu, Zn, Ge, and S are present and their atomic ratios are approximately 2 : 1 : 2 : 6, which is also consistent with the results obtained from single crystal structure determination.

Fig. 2(a) shows the synthesized powder XRD pattern and the simulated pattern of $Eu_2ZnGe_2OS_6$; the two highly similar curves imply the phase purity of the synthesized polycrystalline powder. The IR spectrum of $Eu_2ZnGe_2OS_6$, as depicted in Fig. S3,† exhibits no discernible absorption peaks within the 400–4000 cm^{-1} range. The experimental optical band gap for $Eu_2ZnGe_2OS_6$ was extrapolated to 2.22 eV through the UV-vis-NIR diffuse reflectance data, which is larger than that of commercially available IR NLO crystals AGSe (1.73 eV)[40] and ZGP (2.02 eV),[41] suggesting that the title compound may exhibit a larger LIDT (Fig. 2(b)). Furthermore, the Raman spectrum of a hand-picked small orange-colored blocky crystal of $Eu_2ZnGe_2OS_6$ is plotted in the range of 100–500 cm^{-1} (Fig. S4†), from which several shifts can be observed. The most vigorous Raman shift located at 395 cm^{-1} is generated by the Ge–S vibration of $Eu_2ZnGe_2OS_6$, from which the peaks at 303 and 451 cm^{-1} are also derived. The peak of lower intensity at 257 cm^{-1} generally originates from Zn–S vibration. In addition, the peaks below 200 cm^{-1} (including 163 cm^{-1}) may be attributed to Eu–S vibrations.[42–45]

Considering that $Eu_2ZnGe_2OS_6$ crystallizes in the NCS tetragonal space group $P\bar{4}2_1m$ (no. 113), the SHG test was carried out using a laser with a wavelength of 2090 nm and AGS microcrystals as standard samples, as illustrated in Fig. 2(c). It can be seen that the SHG intensity of $Eu_2ZnGe_2OS_6$ increases with increasing particle size, which indicates that $Eu_2ZnGe_2OS_6$ can achieve type-I PM properties. Moreover, when the particle size is in the range of 125–150 μm, $Eu_2ZnGe_2OS_6$ exhibits a moderate SHG intensity, which is about 0.4 times that of AGS (Fig. 2(d)). In the comprehensive analysis of all the compounds within the $A_2MM'_2OS_6$ system, it is observed that no selenides are

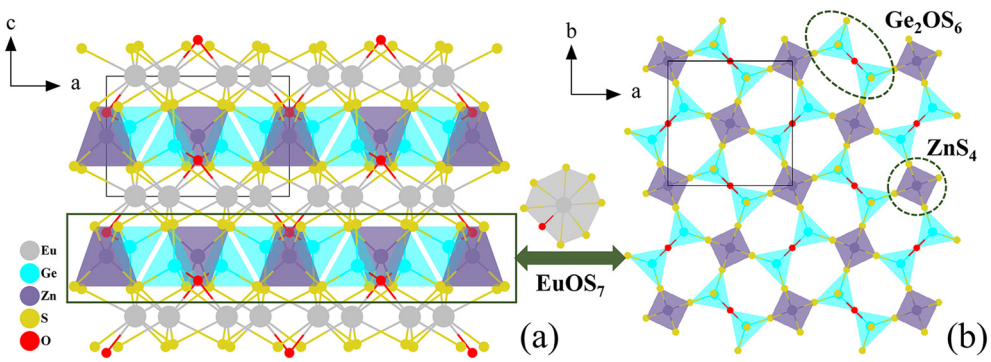

Fig. 1 (a) Crystal structure of $Eu_2ZnGe_2OS_6$ viewed from the *b*-axis; (b) 2D $[ZnGe_2OS_6]^{4-}$ layer viewed along the *ab*-plane.

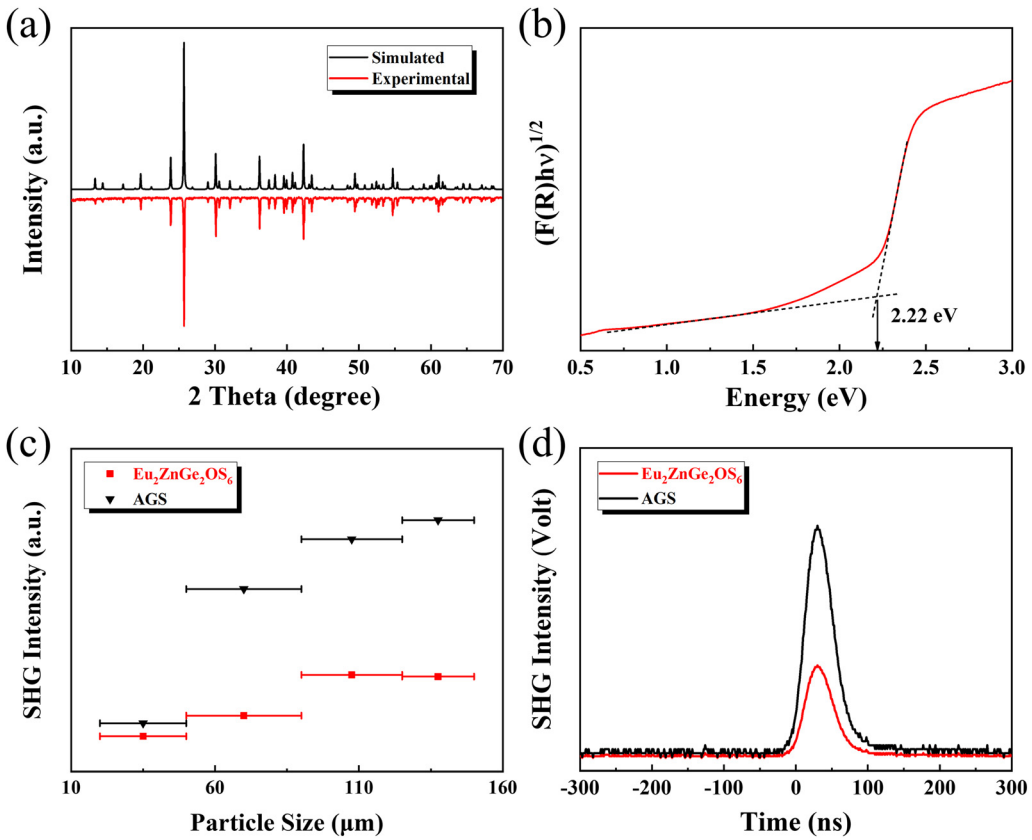

Fig. 2 (a) Experimental and simulated powder XRD patterns and (b) UV-vis-NIR diffuse reflectance spectrum of $Eu_2ZnGe_2OS_6$; (c) SHG intensity *versus* particle size of $Eu_2ZnGe_2OS_6$ and AGS; (d) oscilloscope traces of SHG signals of $Eu_2ZnGe_2OS_6$ and AGS (125–150 μm).

present. Notably, selenides are often characterized by larger SHG coefficients and superior NLO properties compared to sulfides. Consequently, for $Eu_2ZnGe_2OS_6$, rational chemical substitution may emerge as a potential strategy to enhance the NLO performance, such as the substitution of S with Se, the substitution of Ge with heavier Sn, and the substitution of Zn with other heavier d^{10} atoms (*e.g.*, Cd and Hg).

As depicted in Fig. 3(a), $Eu_2ZnGe_2OS_6$ exhibits an indirect band gap of 1.81 eV, with the conduction band (CB) minimum situated at the Γ point and the valence band (VB) maximum situated at the M point. This theoretical band gap is slightly lower than the experimentally determined value of 2.22 eV, which can be attributed to the limitations of the local density approximation (LDA) function when employed in DFT calculations. The LDA function often underestimates the band gap due to its inability to accurately account for the exchange–correlation potential, particularly the discontinuity in the derivative of the exchange–correlation energy concerning the electron density.[46–48] The analysis of the total and partial density of states (TDOS and PDOS) as depicted in Fig. 3(b) reveals that the S 3p orbitals are the predominant contributors to the VB maximum, with a minor incorporation of Eu 4f and 5d orbitals. Similarly, the CB minimum is largely influenced by the S 3p and Ge 4s orbitals, complemented by contributions from the Zn 4s orbitals. This suggests that the optical characteristics of $Eu_2ZnGe_2OS_6$ are predominantly governed by the $[ZnS_4]$ tetrahedron and $[GeOS_3]$ groups. Moreover, the intermixing of Eu 4f orbitals could potentially introduce extra electronic transition pathways, which may subsequently influence the optical properties of $Eu_2ZnGe_2OS_6$. Birefringence (Δn), the difference in refractive index at a specific wavelength, is a characteristic unique to anisotropic crystal systems. It is a pivotal property for functional optical crystals, as it significantly influences angular PM and the ability to adjust the polarization of light. Achieving PM is not possible if the nonlinear optical material's birefringence is too low; thus, a moderate birefringence is necessary for a substantial SHG response.[49–52] The birefringence of $Eu_2ZnGe_2OS_6$ has been calculated to be 0.173 at 2090 nm, a value substantial enough to facilitate PM behavior. This finding is also consistent with the results obtained from the powder SHG tests. Additionally, the dipole moment (DM) analysis of the $[GeOS_3]$ unit and the $[ZnS_4]$ tetrahedron was conducted utilizing the bond valence method.[53] It is evident that the DM of the $[GeOS_3]$ unit substantially exceeds that of the $[ZnS_4]$ tetrahedron, as detailed in Table S4.† This significant difference in DM suggests that the $[GeOS_3]$ unit plays a predominant role in the substantial birefringence observed in $Eu_2ZnGe_2OS_6$.

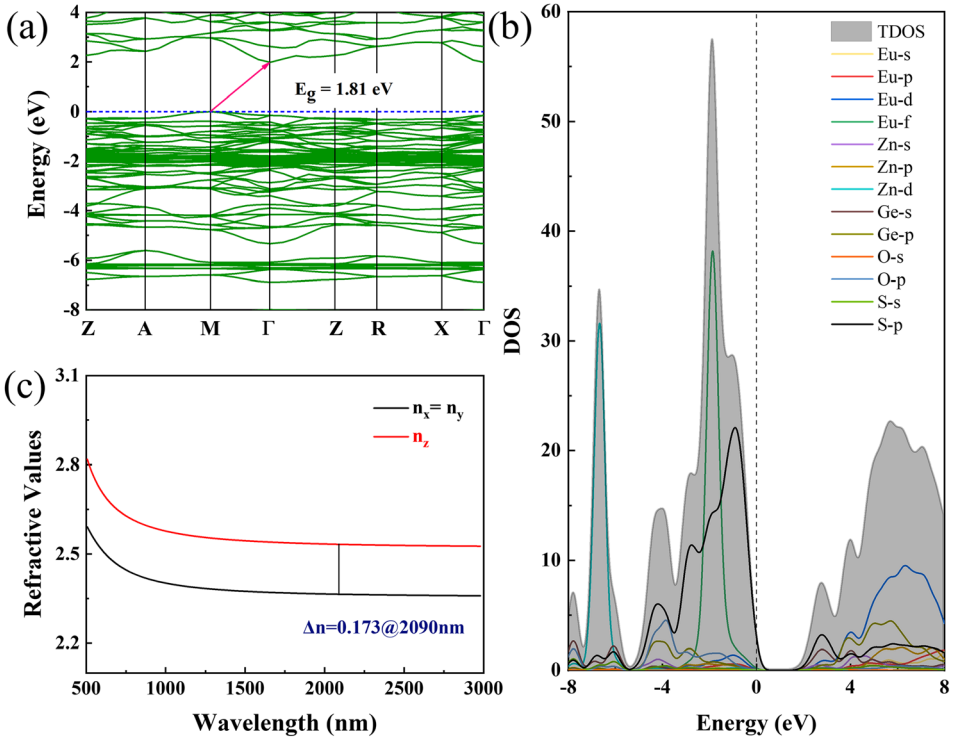

Fig. 3 The calculated results of $Eu_2ZnGe_2OS_6$: (a) electronic band structure, (b) DOS, and (c) birefringence.

Conclusion

In conclusion, a new rare-earth oxychalcogenide $Eu_2ZnGe_2OS_6$ was successfully designed and synthesized, which crystallizes in the NCS $P\bar{4}2_1m$ space group, featuring highly polarized mixed-anion $[GeOS_3]$ units. The title compound exhibits an experimentally determined indirect band gap of 2.22 eV, a modest SHG response (0.4 × AGS), and PM properties. Rational chemical substitution strategies are anticipated to enhance the NLO properties further. This study enriches the rarely studied rare-earth oxychalcogenide system and offers new insights for the design of promising oxychalcogenide IR NLO crystals.

Data availability

The data supporting this article have been included as part of the ESI.† Crystallographic data for $Eu_2ZnGe_2OS_6$ has been deposited at the CCDC under 2390087.

Author contributions

G. L. Wang prepared the samples, designed and conducted the experiments, and wrote the original draft of the manuscript; W. T. Wu performed theoretical calculations; C. X. Li helped with powder SHG tests. J. Y. Yao reviewed and edited the manuscript. All authors reviewed and approved the final form of the submitted manuscript.

Conflicts of interest

There are no conflicts to declare.

Acknowledgements

Thanks for the support of the National Natural Science Foundation of China (no. 22175190).

References

1 D. Pestov, X. Wang, G. O. Ariunbold, R. K. Murawski, V. A. Sautenkov, A. Dogariu, A. V. Sokolov and M. O. Scully, *Proc. Natl. Acad. Sci. U. S. A.*, 2008, **105**, 422–427.
2 V. A. Serebryakov, É. V. Boĭko, N. N. Petrishchev and A. V. Yan, *J. Opt. Technol.*, 2010, **77**, 6–17.
3 A. Abudurusuli, J. Li and S. Pan, *Dalton Trans.*, 2021, **50**, 3155–3160.
4 M. Sun, W. Xing, S. K. Chen, C. Li, W. Liu, M.-H. Lee and J. Yao, *Chem. Mater.*, 2023, **35**, 7218–7228.
5 C. Li, X. Meng, Z. Li and J. Yao, *Coord. Chem. Rev.*, 2022, **453**, 214328.
6 I. Chung and M. G. Kanatzidis, *Chem. Mater.*, 2014, **26**, 849–869.
7 W. Huang, L. Gan, H. Li, Y. Ma and T. Zhai, *CrystEngComm*, 2016, **18**, 3968–3984.
8 D. Eimerl, *Ferroelectrics*, 1987, **72**, 95–139.
9 F. C. Zumsteg, J. D. Bierlein and T. E. Gier, *J. Appl. Phys.*, 2008, **47**, 4980–4985.
10 C. Chen, Y. Wu, A. Jiang, B. Wu, G. You, R. Li and S. Lin, *J. Opt. Soc. Am. B*, 1989, **6**, 616–621.

11 D. N. Nikogosyan, *Appl. Phys. A: Mater. Sci. Process.*, 1991, **52**, 359–368.
12 Y. Wu, T. Sasaki, S. Nakai, A. Yokotani, H. Tang and C. Chen, *Appl. Phys. Lett.*, 1993, **62**, 2614–2615.
13 Y. Mori, I. Kuroda, S. Nakajima, T. Sasaki and S. Nakai, *Appl. Phys. Lett.*, 1995, **67**, 1818–1820.
14 Y. Xia, C. Chen, D. Tang and B. Wu, *Adv. Mater.*, 1995, **7**, 79–81.
15 Y. Sang, D. Yu, M. Avdeev, R. Piltz, N. Sharma, N. Ye, H. Liu and J. Wang, *CrystEngComm*, 2012, **14**, 6079–6084.
16 G. Boyd, H. Kasper, J. McFee and F. Storz, *IEEE J. Quantum Electron.*, 1972, **8**, 900–908.
17 D. S. Chemla, P. J. Kupecek, D. S. Robertson and R. C. Smith, *Opt. Commun.*, 1971, **3**, 29–31.
18 G. D. Boyd, E. Buehler and F. G. Storz, *Appl. Phys. Lett.*, 1971, **18**, 301–304.
19 A. H. Akiko Harasaki and K. K. Kiyoshi Kato, *Jpn. J. Appl. Phys.*, 1997, **36**, 700.
20 G. C. Catella, L. R. Shiozawa, J. R. Hietanen, R. C. Eckardt, R. K. Route, R. S. Feigelson, D. G. Cooper and C. L. Marquardt, *Appl. Opt.*, 1993, **32**, 3948–3951.
21 H. Zhang, M. Zhang, S. Pan, X. Dong, Z. Yang, X. Hou, Z. Wang, K. B. Chang and K. R. Poeppelmeier, *J. Am. Chem. Soc.*, 2015, **137**, 8360–8363.
22 W. Li, L. Geng, C. Meng, S. Ma, B. Zhu, Y. Lan and Q. Wu, *Adv. Opt. Mater.*, 2024, **12**, 2302560.
23 J. Wang, H. Wu, H. Yu, Z. Hu, J. Wang and Y. Wu, *Adv. Opt. Mater.*, 2022, **10**, 2102673.
24 P.-F. Liu, Y.-Y. Li, Y.-J. Zheng, J.-S. Yu, R.-H. Duan, H. Chen, H. Lin, L. Chen and L.-M. Wu, *Dalton Trans.*, 2017, **46**, 2715–2721.
25 L. T. Menezes, E. Gage, A. Assoud, M. Liang, P. S. Halasyamani and H. Kleinke, *Chem. Mater.*, 2023, **35**, 3033–3040.
26 M.-Y. Ran, Z. Ma, H. Chen, B. Li, X.-T. Wu, H. Lin and Q.-L. Zhu, *Chem. Mater.*, 2020, **32**, 5890–5896.
27 M.-Y. Ran, S.-H. Zhou, X.-T. Wu, H. Lin and Q.-L. Zhu, *Mater. Today Phys.*, 2024, **44**, 101442.
28 R. Wang, F. Liang, X. Liu, Y. Xiao, Q. Liu, X. Zhang, L.-M. Wu, L. Chen and F. Huang, *ACS Appl. Mater. Interfaces*, 2022, **14**, 23645–23652.
29 T. Endo, Y. Doi, M. Wakeshima, K. Suzuki, Y. Matsuo, K. Tezuka, T. Ohtsuki, Y. J. Shan and Y. Hinatsu, *Inorg. Chem.*, 2017, **56**, 2459–2466.
30 M.-Y. Ran, S.-H. Zhou, B. Li, W. Wei, X.-T. Wu, H. Lin and Q.-L. Zhu, *Chem. Mater.*, 2022, **34**, 3853–3861.
31 H.-D. Yang, S.-H. Zhou, M.-Y. Ran, X.-T. Wu, H. Lin and Q.-L. Zhu, *Inorg. Chem. Front.*, 2023, **10**, 2030–2038.
32 N. Zhang, Q.-T. Xu, Z.-H. Shi, M. Yang and S.-P. Guo, *Inorg. Chem.*, 2022, **61**, 17002–17006.
33 X. Tian, X. Zhang, Y. Xiao, X. Wu, B. Zhang, D. Yang and K. Wu, *RSC Adv.*, 2022, **12**, 16296–16300.
34 Y. Cheng, H. Wu, H. Yu, Z. Hu, J. Wang and Y. Wu, *Chem. Sci.*, 2022, **13**, 5305–5310.
35 N. Zhang, X. Huang, W.-D. Yao, Y. Chen, Z.-R. Pan, B. Li, W. Liu and S.-P. Guo, *Inorg. Chem.*, 2023, **62**, 16299–16303.
36 G. Wang, C. Li, M.-H. Lee and J. Yao, *Inorg. Chem.*, 2024, **63**, 10288–10295.
37 K. Tezuka, Y. Tokuhara, M. Wakeshima, Y. J. Shan, H. Imoto and Y. Hinatsu, *Inorg. Chem.*, 2013, **52**, 12972–12979.
38 W. Xing, N. Wang, Y. Guo, Z. Li, J. Tang, K. Kang, W. Yin, Z. Lin, J. Yao and B. Kang, *Dalton Trans.*, 2019, **48**, 17620–17625.
39 S. Cui, H. Wu, Z. Hu, J. Wang, Y. Wu and H. Yu, *Adv. Sci.*, 2023, **10**, 2204755.
40 G. A. Babu, R. S. Raja, P. Ramasamy and N. Karunagaran, *AIP Conf. Proc.*, 2012, **1447**, 1045–1046.
41 X. Zhao, S. Zhu, B. Zhao, B. Chen, Z. He, R. Wang, H. Yang, Y. Sun and J. Cheng, *J. Cryst. Growth*, 2008, **311**, 190–193.
42 K. Wu, X. Su, Z. Yang and S. Pan, *Dalton Trans.*, 2015, **44**, 19856–19864.
43 H. Wang, X. Pan, W. Zhao, Y. Chu and J. Li, *Inorg. Chem. Front.*, 2023, **10**, 6253–6261.
44 H. Ben Yahia, K. Motohashi, S. Mori, A. Sakuda and A. Hayashi, *J. Alloys Compd.*, 2023, **960**, 170600.
45 C. Power, E. Moreno, E. Quintero, D. Rivero, M. Quintero, C. Rincón, J. A. Henao and M. A. Macías, *Phys. Status Solidi B*, 2016, **253**, 335–339.
46 J. P. Perdew, *Int. J. Quantum Chem.*, 1986, **30**, 451.
47 D. Koller, F. Tran and P. Blaha, *Phys. Rev. B: Condens. Matter Mater. Phys.*, 2011, **83**, 195134.
48 R. W. Godby, M. Schlüter and L. J. Sham, *Phys. Rev. B: Condens. Matter Mater. Phys.*, 1987, **36**, 6497–6500.
49 X. Chen, Y. Li, J. Luo and S. Zhao, *Chin. J. Struct. Chem.*, 2023, **42**, 100044.
50 Y. Li, Q. Wu, Z. Lin, Y. Liu, Y. Zhou, X. Chen, M. Li, M. Hong, J. Luo and S. Zhao, *Fundam. Res.*, 2023, **3**, 974–978.
51 T. Ouyang, Y. Shen and S. Zhao, *Chin. J. Struct. Chem.*, 2023, **42**, 100024.
52 Y. Zhao, L. Zhu, Y. Li, X. Kuang, J. Luo and S. Zhao, *Mater. Chem. Front.*, 2023, **7**, 3986–3993.
53 P. A. Maggard, T. S. Nault, C. L. Stern and K. R. Poeppelmeier, *J. Solid State Chem.*, 2003, **175**, 27–33.